RSC Advances

PAPER

View Article Online
View Journal | View Issue

Cite this: *RSC Adv.*, 2019, **9**, 18271

Facile stabilization of a cyclodextrin metal–organic framework under humid environment *via* hydrogen sulfide treatment†

Duo Ke,[ac] Jun-Feng Feng,[a] Di Wu,[b] Jun-Bo Hou,[b] Xiao-Qin Zhang,[b] Bang-Jing Li *[a] and Sheng Zhang*[b]

Received 25th April 2019
Accepted 2nd June 2019

DOI: 10.1039/c9ra03079d

rsc.li/rsc-advances

Increasing resistance to humid environments is a major challenge for the application of γ-CD-K-MOF (a green MOF) in real-world utilisation. γ-CD-K-MOF–H_2S with enhanced moisture tolerance was obtained by simply treating MOF with H_2S gas. XPS, Raman and TGA characterizations indicated that the H_2S molecules coordinated with the metal centers in the framework. H_2S acting as a newly available water adsorption potential well near the potassium centers protects the metal–ligand coordination bond from attack by water molecules and thus improves the moisture stability of MOF. After 7 days exposure in 60% relative humidity, γ-CD-K-MOF–H_2S retained its crystal structure and morphology, while γ-CD-K-MOF had nearly collapsed. In addition, the formaldehyde uptake tests indicated that γ-CD-K-MOF retain their permanent porosity after interaction with H_2S. This simple and facile one-step strategy would open a new avenue for preparation of moisture stable MOFs for practical applications.

Introduction

Metal–Organic Frameworks (MOFs), a new class of porous and crystalline materials synthesized by the assembly of organic ligands with metal ions have gained remarkable interest in recent years due to their ultrahigh surface areas, adjustable chemical functionality, and structural diversity.[1–4] MOFs can be reasonably designed and prepared to satisfy desired versatile applications including catalysis,[5] gas storage,[6,7] separation,[8] drug delivery,[9] sensing,[10,11] imaging[12] and proton conductors.[13,14] Their actual implementation depends on the stability of these materials against the environment. Unfortunately, most previously reported MOFs with weak metal–ligand coordination bonds are generally vulnerable to water molecules and collapse in humid and aqueous environments, which severely limit their practical application.[15–17] However, the strategies employed to enhance the moisture resistance of MOFs have been addressed in a few studies. Currently, two main approaches have been developed to improve the water stability of MOFs. One is to directly synthesize stable MOFs by changing the chemical composition of the MOFs to increase the metal–linker bond strengths.[18,19] However, this method is limited to the preparation of new materials, and does not permit enhancing the stability of those already available. The other effective method involves post-synthetic modifications, such as encapsulation of hydrophobic guest molecules,[20,21] modification of the linkers with hydrophobic groups[22–24] and functionalization of their external surfaces *via* hydrophobic coatings[25–27] to protect the MOFs from water intrusion. Despite successful improving the water stability of MOFs, these approaches suffered from their respective limitations, including tedious procedure, complex instrumentation and reduced the functionality of materials.

Recently, γ-cyclodextrin based MOF (γ-CD-K-MOF), which linked by coordination of the hydroxyl groups on γ-cyclodextrin with potassium ions to form body-centered cubic structure,[28] have attracted broad attention. The six γ-CD units are combined by the coordination of K^+ ions with C_6 OH groups and glycosidic ring oxygen atoms of D-glucopyranosyl residues on the primary face of the γ-CD to formed $(\gamma\text{-CD})_6$ cube. The $(\gamma\text{-CD})_6$ cubes are attached to one another by the coordination of K^+ ions to the C_2 and C_3 OH groups of the other set of alternating residues on the secondary face of the γ-CD to formed 3D extended frameworks. The γ-CD-K-MOF shows two main kinds of pores: spherical voids with diameters 1.7 nm and apertures with diameter 0.78 nm.[29] Due to the porous structure, high local concentration of the hydroxyl groups and biocompatibility, this γ-CD-K-MOF holds prospective applications in gas adsorption,[30] small molecules separation,[31] sensing[32,33] and biomedicine.[34,35] In particular, the adsorption of toxic gases from breathable air for personal protection is an excellent example of MOFs in practical

[a]*Key Laboratory of Mountain Ecological Restoration and Bioresource Utilization, Chengdu Institute of Biology, Chinese Academy of Sciences, Chengdu 610041, China. E-mail: libj@cib.ac.cn*

[b]*State Key Laboratory of Polymer Materials Engineering (Sichuan University), Polymer Research Institute of Sichuan University, Chengdu 610065, China. E-mail: zslbj@163.com*

[c]*University of Chinese Academy of Sciences, Beijing 100049, China*

† Electronic supplementary information (ESI) available. See DOI: 10.1039/c9ra03079d

applications. Previously, our group have demonstrated that γ-CD-K-MOF showed high selective adsorption capability and speed for formaldehyde owing to the host–guest interactions between γ-CD and HCHO and hydrogen bonding with hydroxyl groups.[36] However, these applications face severe challenges associated with the poor stability of γ-CD-K-MOF, which rapidly decomposed when in contact with moisture. Up to now, only few studies have been reported for the improvement of moisture stability of γ-CD-K-MOF. One is to obtain water insoluble γ-CD-K-MOF by cross-linking γ-CD with crosslinkers such as diphenyl carbonate or ethylene glycol diglycidyl.[37,38] However, the synthesis and post-processing were complicated and time-consuming. Li *et al.* incorporated fullerene (C_{60}) in the γ-CD-K-MOF matrices, the exposed surface of the trapped C_{60} imparted the γ-CD-K-MOF with enhanced hydrophobicity to improve their water stability.[39] However, the occupancy of γ-CD cavities by C_{60} might reduce the capacity of γ-CD-K-MOF to load drugs. Recently, Singh *et al.* grafted a layer of hydrophobic cholesterol on the external surface of γ-CD-K-MOF.[40] The water resistance of the functionalized MOF is higher than the bare MOF, while such chemistry modification was also time-consuming (taking 24 h at 45 °C) and used organic solvent *N*,*N*-dimethyl formamide. Thus, it is still an urgent need to develop more facile and efficient strategies to improve the moisture resistance of γ-CD-K-MOF.

In this work, we report a very simple and efficient method to enhance the humidity tolerance of γ-CD-K-MOF by treating the γ-CD-K-MOF with hydrogen sulfide (H_2S) atmosphere. Unlike other strategies employed to enhance the moisture resistance of MOFs, H_2S stabilized γ-CD-K-MOF through coordinating with potassium metal sites and as new basins of attraction for the incoming water molecules, thus depleting the water content at the metal centers and improving its moisture resistance. It was found that H_2S coordinated γ-CD-K-MOF remained the ability to rapidly adsorb formaldehyde and formaldehyde uptake capacity. To the best of our knowledge, this is the first work that improves moisture resistance of MOF *via* a facile gas treatment.

Experimental section

Materials and methods

γ-Cyclodextrin (99%), ferrous sulphide and barium hydroxide, cetyltrimethylammonium bromide (CTAB) were purchased from Sigma-Aldrich (Shanghai China). Potassium hydroxide (KOH), formaldehyde (HCHO), methyl alcohol and ethyl alcohol were produced from Chengdu Kelong Chemical Engineering Company (Chengdu China). All other reagents were of analytical grade and were used directly without further purification.

Characterization

Scanning electron microscope (SEM) measurements were performed with Phenom pro, Phenom-world BV. X-Ray powder diffraction (XRD) data was collected on Panalytical B.V at room temperature from 3° to 40° (2θ). Thermal studies were conducted with Thermal Analyzer EXSTAR 6000 (Seiko Instruments Inc, Japan) in the temperature ranging 30–600 °C with heating rates of 10 °C min^{-1} under a N_2 atmosphere. The FT-IR results were determined in Thermo Fisher Scientific Nicolet 6700 in the wavenumber range of 4000–400 cm^{-1}. The Raman spectra were recorded using a Renishaw Raman Microscope spectrometer with laser emitting at 532 nm. The X-ray photoelectron spectroscopy (XPS) was carried on Thermo VG Multilab 2000 with Al Kα radiation in an ultra-high vacuum. The contact angle (CA) of water was measured at RT by using a CA meter (Data Physics, OCA20). Sessile water drops of 3 μL were used, and the value reported here was the average of three different positions.

Synthesis of γ-CD-K-MOF. The γ-CD (324 mg) was mixed with KOH (112 mg) in pure water (10 mL). 1 mL MeOH was added, followed by vapor diffusion of MeOH into the solution at 50 °C. After 6 h, the supernatant was transferred into another glass tube with addition of CTAB (8 mg mL^{-1}) and 10 mL MeOH, and then the solution was incubated at room temperature for 5 h. Finally, the precipitate was washed with isopropanol and dried overnight at 50 °C under vacuum.

Fabrication of H_2S-coordinated γ-CD-K-MOF. An amount of γ-CD-K-MOF was sealed in a flask. The sample flask was first evacuated to remove the gas and then back-filled with hydrogen sulfide to a final pressure of 1 atm. The flask with the γ-CD-K-MOF was kept under this saturated H_2S atmosphere for 24 h, and then the γ-CD-K-MOF loaded with H_2S was heated at 50 °C under vacuum for 2 days to remove H_2S gas physically adsorbed in the γ-CD-K-MOF pores and the γ-CD-K-MOF coordinated with H_2S was obtained.

Solubility experiment. The γ-CD-K-MOF solved in the water would release γ-CD. Thus, the solubility of γ-CD-K-MOF was quantified by measured the amount of γ-CD in the aqueous solution. The γ-CD content was measured from the change of absorbance based on the host–guest interactions between the γ-CD and *o*-cresolphthalein. A defined amount of γ-CD-K-MOF was weighed and placed in a flask respectively, and then added 5 mL water by ultrasound to make a series of solutions from unsaturated to supersaturated. After setting for 24 h, the supernatant was filtered and added *o*-cresolphthalein solution. Lastly, the absorbance values were measured at 567 nm after stay in a water bath at 30 °C for 15 min.

Study on formaldehyde adsorption behaviour of materials. (1) Formaldehyde adsorption test. A defined amount of materials and portable formaldehyde detector were put into vacuum-tight container and the formaldehyde solution (the concentration was 0.6%) was added. Then, electrical heater was used to heat formaldehyde solution and convert formaldehyde into gaseous form. Portable formaldehyde detector was applied to monitor the change of formaldehyde concentration at 293 K and 1 atm. (2) Formaldehyde saturated adsorption test. A defined amount of materials was placed in a dry saturated formaldehyde steam condition for 2 days, and the saturated adsorption capacity of materials was calculated by comparing the weight before and after the formaldehyde adsorption.

Results and discussion

The H_2S stabilized γ-CD-K-MOF was simply conducted *via* absorption of H_2S. After absorption, the γ-CD-K-MOF loaded

with H_2S was heated at 50 °C under vacuum for 2 days to remove physically adsorbed H_2S gas. For the convenience of our discussion, we use the notation γ-CD-K-MOF–H_2S and γ-CD-K-MOF/H_2S to refer to the H_2S-loaded γ-CD-K-MOF with and without degassing respectively.

The powder X-ray diffraction (XRD) patterns of γ-CD-K-MOF–H_2S were identical to that of the parent γ-CD-K-MOF (Fig. S1†),[28] indicating that γ-CD-K-MOF–H_2S and γ-CD-K-MOF have the same crystalline structure. The X-ray photoelectron spectroscopy (XPS) proved the presence of S in γ-CD-K-MOF–H_2S after γ-CD-K-MOF loaded with H_2S degassed under vacuum at 323 K, indicating that H_2S is bound to the framework of γ-CD-K-MOF through some interactions (Fig. 1a). The binding energy of K 2p in γ-CD-K-MOF–H_2S exhibited an obvious shift to low binding energy compared to γ-CD-K-MOF, revealing the possible coordination bond formation between the K centers and S atoms from the H_2S. In terms of S 2p, the peak (161.3 eV) assigned to S–K bond (Fig. S2†).[41] It is reasonable to consider that H_2S was coordinated to K metal ions in frameworks rather than agglomerating inside γ-CD-K-MOF pores or replacing γ-CD ligands and compromising its porous structure.

Thermogravimetric (TG) analysis was performed on γ-CD-K-MOF and γ-CD-K-MOF–H_2S and the results were shown in Fig. S3.† It is observed that pristine γ-CD-K-MOF has a mass loss of 8.8% at low temperature and then is stable to temperatures as high as 200 °C. The γ-CD-K-MOF–H_2S showed two mass losses, a 4.5% mass loss at low temperatures similarly to pristine γ-CD-K-MOF followed by a gradual mass loss at higher temperature (120–200 °C), which might be assigned to H_2S coordinated to the γ-CD-K-MOF. From TG analysis it was estimated an 8% H_2S coordinated to the metal ions of γ-CD-K-MOF.

Fig. 1b compared the Raman spectrum of the γ-CD-K-MOF and γ-CD-K-MOF–H_2S. The bare γ-CD-K-MOF exhibited two bands centred at 438 and 478 cm^{-1}, which shifted to 442 and 475 cm^{-1} respectively upon H_2S interaction. At lower frequency, the additional component, observed at 374, 217 and 149 cm^{-1} and absent in both pristine γ-CD-K-MOF and γ-CD-K-MOF–H_2S heated under vacuum at 130 °C for 7 h (coordinated H_2S would be released at 130 °C according to TGA profiles), could be associated to the vibration of the K–S bond of the coordinated H_2S. The above results demonstrated that H_2S was coordinated to the potassium ion in the γ-CD-K-MOF.

Interestingly, the moisture stability of γ-CD-K-MOF was significantly enhanced after interaction with H_2S. The moisture resistance of pristine γ-CD-K-MOF and γ-CD-K-MOF–H_2S were investigated with exposure to air at 60% relative humidity for 7 days. As shown in Fig. 2, the morphology and structure of all the samples were monitored by scanning electron microscopy (SEM) and XRD respectively. SEM image showed that γ-CD-K-MOF lost its cubic shapes and the edges become rounder after staying in humid environment for 7 days (Fig. 2a and b). In sharp contrast, the γ-CD-K-MOF–H_2S showed the identical morphology before and after the 7 days treatment in humid environment (Fig. 2d and e). Powder XRD results showed that the characteristic peaks at 4.1°, 5.7° and 7.0° for the γ-CD-K-MOF disappeared and the peak broaden at 16.4° after treated in humidity (RH 60%) for 7 days, revealing the destruction of the initial structure. In contrast, the framework and crystallinity of γ-CD-K-MOF–H_2S retained after the same treatment. In addition, treatment of γ-CD-K-MOF and γ-CD-K-MOF–H_2S at higher humidity of 92% RH for 5 days, SEM images showed that the cubic crystals of γ-CD-K-MOF collapsed completely, while γ-CD-K-MOF–H_2S remained regular cubic shape (Fig. S4†). The above results unambiguously demonstrated that the coordination of H_2S on γ-CD-K-MOF effectively improved its moisture resistance.

Contact angle provided quantitative information on the wettability of the solid surface. For powder materials, the measured contact angle is usually smaller due to the roughness and porosity of the pellets produced.[42] Therefore, to provide approximate estimation of the hydrophobic/hydrophilic characteristics of γ-CD-K-MOF and γ-CD-K-MOF–H_2S, the measured sample was obtained by applying pressure (under 1 Mpa for 30 s). As shown in Fig. 3, the water contact angle for γ-CD-K-MOF is 16 ± 1°. After the H_2S treatment, the corresponding γ-CD-K-MOF–H_2S exhibited a water contact angles as 38 ± 1°, which are more than twice with respect to γ-CD-K-MOF. These results confirmed that γ-CD-K-MOF become more hydrophobic after coordinated to H_2S.

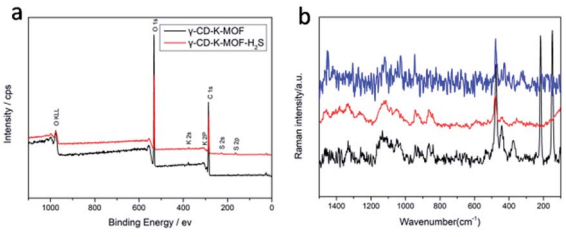

Fig. 1 (a) XPS spectra of γ-CD-K-MOF and γ-CD-K-MOF–H_2S (b) Raman spectra of the γ-CD-K-MOF (red), γ-CD-K-MOF–H_2S (black) and γ-CD-K-MOF–H_2S heated under vacuum at 130 °C for 7 h (blue).

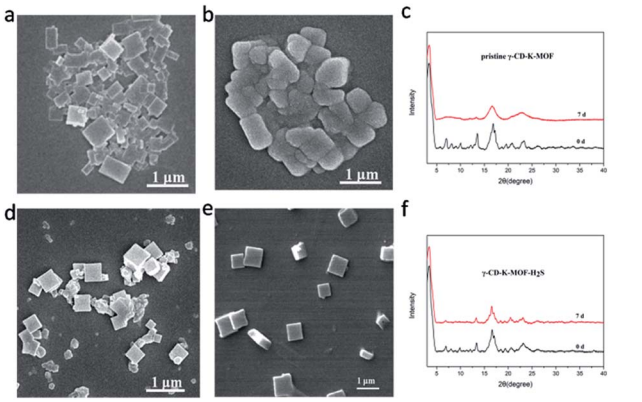

Fig. 2 SEM image of pristine γ-CD-K-MOF (a) before and (b) after exposure to humidity (RH 60%) for 7 days. SEM image of γ-CD-K-MOF–H_2S (d) before and (e) after exposure to humidity (RH 60%) for 7 days. Powder XRD patterns of pristine γ-CD-K-MOF (c) and γ-CD-K-MOF–H_2S (f) before and after exposure to humidity (RH 60%) for 7 days.

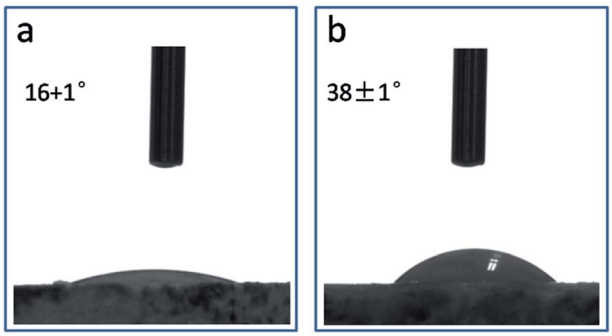

Fig. 3 The water contact angle of (a) γ-CD-K-MOF (b) γ-CD-K-MOF–H_2S.

The water adsorption capacity of γ-CD-K-MOF and γ-CD-K-MOF–H_2S was performed on exposure to a moist environment at 298 K. γ-CD-K-MOF showed a rapid increase in mass as the material adsorbs water and no further change over the remainder of the experiment (up to 4 days) (Fig. S5†). The γ-CD-K-MOF–H_2S showed a similar immediate mass gain as the water adsorption, but water uptake significant decrease with respect to γ-CD-K-MOF. These results are in complete agreement with the observed lower solvent loss on γ-CD-K-MOF–H_2S from TGA profiles, which could be attributed to the more hydrophobic features of the γ-CD-K-MOF–H_2S that decrease the incorporation of water molecules inside the framework cavities. In order to get further insight into the improvement of moisture resistance after H_2S coordinated to the γ-CD-K-MOF, we also studied the solubility of γ-CD-K-MOF and γ-CD-K-MOF–H_2S in aqueous solution. Due to the weak metal–ligand coordination, γ-CD-K-MOF decomposes in water and release γ-CD. Thus, the maximum degradation of materials could be quantified by the amount of γ-CD in the solution. The measured concentration of samples that not increased with the addition of samples was taken as the solubility of the tested material. It was found that γ-CD-K-MOF rapidly dissolved in water and showed solubility as large as 76 mg mL^{-1} (Fig. S6†), while γ-CD-K-MOF–H_2S exhibited slow dissolution rate and the solubility is 0.4 mg mL^{-1}. The γ-CD-K-MOF/H_2S also showed lower solubility of 0.3 mg mL^{-1}. The solubility of the γ-CD-K-MOF–H_2S is significantly decreased after interaction with H_2S.

The γ-CD-K-MOF showed extreme sensitivity to moisture because it is believed that the weak potassium–oxygen coordination allows for an attack by water molecules. Water aggregation has been identified as an important prerequisite for some hydrolysis reactions and Fuchs *et al.* demonstrated that metal–ligand coordination bond could be broken after water formed clusters around the metal centers.[43,44] In addition, López *et al.* showed that the introduction of polar groups into the IRMOFs structure could enhance their hydrothermal stability, because the polar functional group as a new adsorption site competed with the metal centers for the adsorption of water molecules so as to effectively prevent the attack from water molecules to the vulnerable coordination bonds.[45] In this study, H_2S molecules bind to the γ-CD-K-MOF by the coordination of H_2S with metal ions. The presence of H_2S endowed γ-CD-K-MOF–H_2S with significantly enhanced moisture stability primarily attributed to the fact that the polar H_2S as a new available water adsorption potential well near the potassium centers draws water away from the metal centers to prevent the formation of water clusters at the potassium site and protect the a vulnerable metal–ligand coordination bonds from the attack of water molecules (Fig. 4). The γ-CD-K-MOF/H_2S showed higher hydrophobicity than γ-CD-K-MOF–H_2S as shown in Fig. S8,† while γ-CD-K-MOF/H_2S exhibited similar solubility to γ-CD-K-MOF–H_2S, which excludes the hydrophobicity of γ-CD-K-MOF–H_2S is mainly responsible for its water stability. This result further demonstrated that the water stability enhancement of γ-CD-K-MOF–H_2S mainly attributed to the coordinated H_2S that preferentially adsorb incoming water molecules to diminish the aggregation of water molecules in metal centers. In addition, the hydrophobicity enhancement of γ-CD-K-MOF–H_2S also contributed to improvement of the moisture resistance.

The data of γ-CD-K-MOF–H_2S BET surface area might be inaccurate since coordinated H_2S might be released during the degassed process of the measurement. Therefore, we investigated the porosities of γ-CD-K-MOF–H_2S by measuring its formaldehyde adsorption capability. It has been demonstrated that γ-CD-K-MOF showed effective formaldehyde adsorption capability.[36] Fig. 5 showed the formaldehyde adsorption behaviour of γ-CD-K-MOF and γ-CD-K-MOF–H_2S. In this study, formaldehyde gas was obtained by heating formaldehyde solution. Taking into account the high-speed formaldehyde adsorption of γ-CD-K-MOF, it is not surprising that the maximum concentration of formaldehyde measured by the formaldehyde detector was lower than theoretical maximum concentration of formaldehyde (2.643 mg m^{-3}), because partial formaldehyde gas has been adsorbed during the heating process. It can be seen that γ-CD-K-MOF–H_2S exhibited similar adsorbing behaviour with γ-CD-K-MOF at this situation,

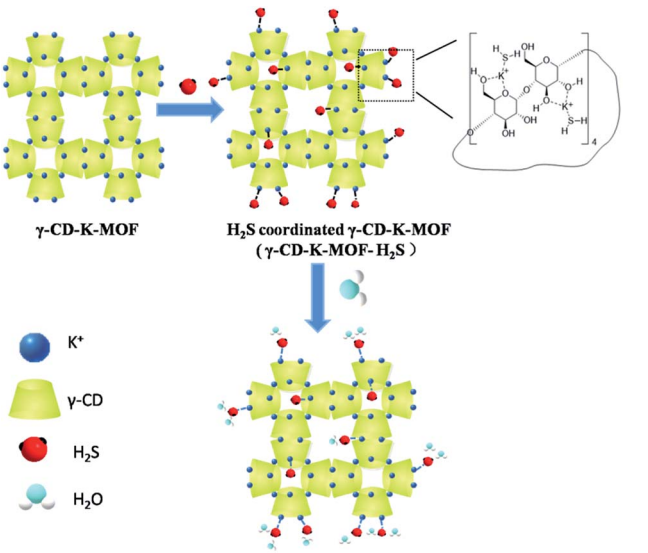

Fig. 4 Schematic illustration of mechanism of improving the moisture resistance of γ-CD-MOF by H_2S treatment.

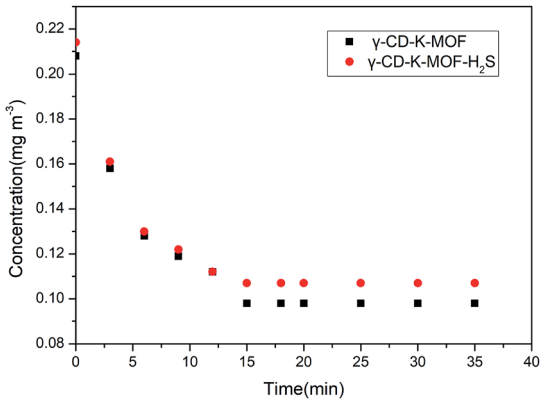

Fig. 5 Formaldehyde adsorption curves of γ-CD-K-MOF and γ-CD-K-MOF–H_2S.

demonstrating that γ-CD-K-MOF remained their permanent porosity after interaction with H_2S.

We also studied their saturated formaldehyde loading capacity. It was found that H_2S treatment makes γ-CD-K-MOF lost around 60% formaldehyde adsorption capacity (Table S1†), which may be since two reasons: (1) it has been reported that hydroxyl groups in γ-CD-K-MOF contribute to formaldehyde adsorption *via* forming hydrogen binds with formaldehyde molecules, but coordinated H_2S form hydrogen bonds with hydroxyl groups firstly and then intervene the formaldehyde adsorption; (2) the coordinated H_2S occupied the some of the pores in the MOF. But it should be noticed that γ-CD-K-MOF–H_2S still showed a formaldehyde adsorption capacity three times higher than that of activated carbon.[36]

Conclusions

In summary, we have reported a facile and efficient strategy to improve moisture stability of γ-CD-K-MOF *via* simple introduction of H_2S. The H_2S coordinated with the potassium ions in the frameworks preferentially adsorb incoming water to diminish water cluster–γ-CD-K-MOF interactions, avoiding the linker displacement. The coordinated H_2S not only greatly enhances MOFs' moisture resistance but also improve its hydrophobicity. When exposed to humid environment (RH = 60%) for 7 days, γ-CD-K-MOF–H_2S retained its crystal structure and morphology, while the as-synthesized γ-CD-K-MOF quickly collapsed. The formaldehyde uptake tests indicated that γ-CD-K-MOF remained its permanent porosity after interaction with H_2S. It is the first time to enhance MOF moisture stability *via* introducing polar gas into the MOFs' structure to form vulnerable coordination bonds. This simply and facile one-step strategy would open a new avenue for preparation of moisture stable MOFs for practical applications.

Conflicts of interest

There are no conflicts to declare.

Acknowledgements

This work was funded by National Natural Science Foundation of China (Grant No. 51573187), the Biological Resources Network of Chinese Academy of Sciences (ZSTH-030) and State Key Laboratory of Polymer Materials Engineering (Grant No. sklpme2017-2-05).

Notes and references

1 F. Hiroyasu, K. E. Cordova, O. K. Michael and O. M. Yaghi, *Science*, 2013, **341**, 974–989.
2 E. Mohamed, K. Jaheon, R. Nathaniel, V. David, W. Joseph, O. K. Michael and O. M. Yaghi, *Science*, 2002, **295**, 469–472.
3 Z. G. Gu, G. Sylvain, B. S. Stefan, W. L. Christof and H. Lars, *Chem. Commun.*, 2015, **51**, 8998–9001.
4 W. G. Lu, Z. W. Wei, Z. Y. Gu, T. F. Liu, P. Jinhee, P. Jihye, T. Jian, M. W. Zhang, Q. Zhang and G. Thomas, *Chem. Soc. Rev.*, 2014, **43**, 5561–5593.
5 L. Jeongyong, O. K. Farha, R. John, K. A. Scheidt, S. B. T. Nguyen and J. T. Hupp, *Chem. Soc. Rev.*, 2009, **38**, 1450–1459.
6 S. Krause, V. Bon, I. Senkovska, U. Stoeck, D. Wallacher, D. M. Többens, S. Zander, R. S. Pillai, G. Maurin and F. X. Coudert, *Nature*, 2016, **532**, 348–352.
7 S. Q. Ma and H. C. Zhou, *Chem. Commun.*, 2010, **46**, 44–53.
8 J. R. Li, K. J. Ryan and H. C. Zhou, *Chem. Soc. Rev.*, 2009, **38**, 1477–1504.
9 T. Simon-Yarza, A. Mielcarek, P. Couvreur and C. Serre, *Adv. Mater.*, 2018, **30**, 1707365–1707380.
10 Z. S. Dou, J. C. Yu, Y. J. Cui, Y. Yang, Z. Y. Wang, D. Yang and G. D. Qian, *J. Am. Chem. Soc.*, 2014, **136**, 5527–5530.
11 X. Zhu, H. Y. Zheng, X. F. Wei, Z. Y. Lin, L. H. Guo, B. Qin and G. N. Chen, *Chem. Commun.*, 2013, **49**, 1276–1278.
12 H. Patricia, C. Tamim, S. Christian, G. Brigitte, S. Catherine, B. Tarek, J. F. Eubank, H. Daniela, C. Pascal and K. Christine, *Nat. Mater.*, 2010, **9**, 172–178.
13 G. K. H. Shimizu, J. M. Taylor and S. R. Kim, *Science*, 2013, **341**, 354–355.
14 R. Padmini, N. E. Wong and G. K. H. Shimizu, *Chem. Soc. Rev.*, 2014, **43**, 5913–5932.
15 H. Sang Soo, C. Seung-Hoon and A. van Duin, *Chem. Commun.*, 2010, **46**, 5713–5715.
16 J. J. Low, A. I. Benin, J. Paulina, J. F. Abrahamian, S. A. Faheem and R. R. Willis, *J. Am. Chem. Soc.*, 2009, **131**, 15834–15842.
17 J. A. Greathouse and M. D. Allendorf, *J. Am. Chem. Soc.*, 2006, **128**, 10678–10679.
18 M. Kandiah, M. H. Nilsen, S. Usseglio, S. Jakobsen, U. Olsbye, M. Tilset, C. Larabi, E. A. Quadrelli, F. Bonino and K. P. Lillerud, *Chem. Mater.*, 2010, **22**, 6632–6640.
19 F. Hiroyasu, G. Felipe, Y. B. Zhang, J. C. Jiang, W. L. Queen, M. R. Hudson and O. M. Yaghi, *J. Am. Chem. Soc.*, 2014, **136**, 4369–4391.
20 S. J. Yang, J. Y. Choi, H. K. Chae, J. H. Cho, K. S. Nahm and R. P. Chong, *Chem. Mater.*, 2009, **21**, 1893–1897.

21 J. B. Decoste, G. W. Peterson, M. W. Smith, C. A. Stone and C. R. Willis, *J. Am. Chem. Soc.*, 2012, **134**, 1486–1489.
22 H. Li, Z. Lin, X. Zhou, X. Wang, Y. Li, H. Wang and Z. Li, *Chem. Eng. J.*, 2017, **307**, 537–543.
23 J. G. Nguyen and S. M. Cohen, *J. Am. Chem. Soc.*, 2010, **132**, 4560–4561.
24 T. Wu, L. Shen, M. Luebbers, C. Hu, Q. Chen, Z. Ni and R. I. Masel, *Chem. Commun.*, 2010, **46**, 6120–6122.
25 J. Castells-Gil, F. Novio, N. M. Padial, S. Tatay, D. Ruíz-Molina and C. Martí-Gastaldo, *ACS Appl. Mater. Interfaces*, 2017, **9**, 44641–44648.
26 Z. Wang, Y. L. Hu, J. Ge, H. L. Jiang and S. H. Yu, *J. Am. Chem. Soc.*, 2014, **136**, 16978–16981.
27 C. S. Arnau, K. C. Stylianou, C. Carlos, N. Majid, I. Inhar and M. Daniel, *Adv. Mater.*, 2015, **27**, 869–873.
28 R. A. Smaldone, R. S. Forgan, H. Furukawa, J. J. Gassensmith, A. M. Z. Slawin, O. M. Yaghi and J. F. Stoddart, *Angew. Chem., Int. Ed.*, 2010, **49**, 8630–8634.
29 R. S. Forgan, R. A. Smaldone, J. J. Gassensmith, H. Furukawa, D. B. Cordes, Q. Li, C. E. Wilmer, Y. Y. Botros, R. Q. Snurr, A. M. Z. Slawin and J. F. Stoddart, *J. Am. Chem. Soc.*, 2012, **134**, 406–417.
30 J. J. Gassensmith, F. Hiroyasu, R. A. Smaldone, R. S. Forgan, Y. Y. Botros, O. M. Yaghi and S. J. Fraser, *J. Am. Chem. Soc.*, 2011, **133**, 15312–15315.
31 K. J. Hartlieb, J. M. Holcroft, P. Z. Moghadam, N. A. Vermeulen, M. M. Algaradah, M. S. Nassar, Y. Y. Botros, R. Q. Snurr and J. F. Stoddart, *J. Am. Chem. Soc.*, 2016, **138**, 2292–2301.
32 J. J. Gassensmith, K. Jeung Yoon, J. M. Holcroft, O. K. Farha, S. J. Fraser, J. T. Hupp and J. Nak Cheon, *J. Am. Chem. Soc.*, 2014, **136**, 8277–8282.
33 D. Shen, G. Wang, Z. Liu, P. Li, K. Cai, C. Cheng, Y. Shi, J. M. Han, C. W. Kung, X. Gong, Q. H. Quo, H. Chen, A. C. H. Sue, Y. Y. Botros, A. Facchetti, O. K. Farha, T. J. Marks and J. F. Stoddart, *J. Am. Chem. Soc.*, 2018, **140**, 11402–11407.
34 W. Michida, M. Ezaki, M. Sakuragi, G. Guan and K. Kusakabe, *Cryst. Res. Technol.*, 2015, **50**, 556–559.
35 K. J. Hartlieb, D. P. Ferris, J. M. Holcroft, I. Kandela, C. L. Stern, M. S. Nassar, Y. Y. Botros and J. F. Stoddart, *Mol. Pharm.*, 2017, **14**, 1831–1839.
36 L. Wang, X. Y. Liang, Z. Y. Chang, L. S. Ding, S. Zhang and B. J. Li, *ACS Appl. Mater. Interfaces*, 2017, **10**, 42–46.
37 V. Singh, T. Guo, L. Wu, J. H. Xu, B. T. Liu, R. Gref and J. W. Zhang, *RSC Adv.*, 2017, **7**, 20789–20794.
38 Y. Furukawa, T. Ishiwata, K. Sugikawa, K. Kokado and K. Sada, *Angew. Chem., Int. Ed.*, 2012, **51**, 10566–10569.
39 H. Li, M. R. Hill, R. Huang, C. Doblin, S. Lim, A. J. Hill, R. Babarao and P. Falcaro, *Chem. Commun.*, 2016, **52**, 5973–5976.
40 V. Singh, T. Guo, H. T. Xu, L. Wu, J. K. Gu, C. B. Wu, R. Gref and J. W. Zhang, *Chem. Commun.*, 2017, **53**, 9246–9249.
41 M. Fantauzzi, B. Elsener, D. Atzei, A. Rigoldi and A. Rossi, *RSC Adv.*, 2015, **5**, 75953–75963.
42 E. Chibowski and R. Perea-Carpio, *Adv. Colloid Interface Sci.*, 2002, **98**, 245–264.
43 B. Luca, C. Juan Manuel, V. Thijs, C. Sofía and L. Núria, *Chem.–Eur. J.*, 2012, **18**, 12260–12266.
44 T. M. De, R. Jonchiere, P. Pullumbi, F. X. Coudert and A. H. Fuchs, *ChemPhysChem*, 2012, **13**, 3497–3503.
45 L. Bellarosa, J. J. Gutiérrez-Sevillano, S. Calerob and N. López, *Phys. Chem. Chem. Phys.*, 2013, **15**, 17696–17704.